frontiers in Earth Science

ORIGINAL RESEARCH
published: 03 December 2021
doi: 10.3389/feart.2021.799935

Holocene Environmental Changes Inferred From an Aeolian-Palaeosol-Lacustrine Profile in the Mu Us Desert, Northern China

Xiaokang Liu[1,2], Ruijie Lu[2], Zhiyong Ding[3], Zhiqiang Lyu[4], Yijing Li[1] and Zhibao Dong[1,5]*

[1]School of Geography and Tourism, Shaanxi Normal University, Xi'an, China, [2]Engineering Center of Desertification and Blown-Sand Control of Ministry of Education, Faculty of Geographical Science, Beijing Normal University, Beijing, China, [3]State Key Laboratory of Geohazard Prevention and Geoenvironment Protection, Chengdu University of Technology, Chengdu, China, [4]Georges Lemaître Centre for Earth and Climate Research, Earth and Life Institute, Université Catholique de Louvain, Ottignies-Louvain-la-Neuve, Belgium, [5]Planetary Aeolian Research Institute, Shaanxi Normal University, Xi'an, China

An excavated profile of aeolian-palaeosol-lacustrine sediments (the Wapianliang profile), located at the southeastern part of the Mu Us Desert, Northern China, was studied to reconstruct regional Holocene environmental changes. A chronology was established based on three AMS ^{14}C and two OSL dates, and variations in the lithology and grain size, magnetic susceptibility, soil micromorphology, and chemical elements were used to explore the regional depositional environments during the Holocene. The results showed that since around 14 ka BP, this region had experienced seven alternations of wetting and drying. A shallow lake, which was identified by celadon lacustrine sediments with sporadic freshwater gastropod fossils, occurred in this area from around 13.0 ka BP to 9.9 ka BP. There existed two obvious intervals of soil formation, inferred from the environmental proxies of the palaeosol/sandy palaeosol layers, with relatively fine average grain-size, high magnetic susceptibility value, remarkable pedogenesis features, and strong chemical weathering, in particular, a well-developed palaeosol layer dating from the middle Holocene (8.6 ka BP to 4.2 ka BP). A weakly-developed palaeosol layer (from around 1.2 ka BP) at the upper part of the profile is possibly an indication of the Medieval Warm Period. This implies a forest steppe environment at both of these sedimentary stages. After 0.9 ka BP, a desert environment returned, analogous to before around 13.0 ± 1.4 ka BP, between 9.9 ± 1.1 ka BP to 8.6 ka BP, and between 4.2 ka BP to 1.6 ka BP, indicating the aggravation of aeolian activity and the expansion of mobile sand dunes. The variations in sedimentary environments were mainly triggered by changes in the East Asian Summer Monsoon (EASM).

Keywords: Mu Us Desert, environmental changes, Holocene, sedimentary condition, East Asian summer monsoon

OPEN ACCESS

Edited by:
Zhuolun Li,
Lanzhou University, China

Reviewed by:
Peixian Shu,
Chinese Academy of Sciences, China
Zhengcai Zhang,
Chinese Academy of Sciences, China

****Correspondence:***
Ruijie Lu
ruijielu@bnu.edu.cn

Specialty section:
This article was submitted to Quaternary Science, Geomorphology and Paleoenvironment, a section of the journal Frontiers in Earth Science

Received: *22 October 2021*
Accepted: *10 November 2021*
Published: *03 December 2021*

Citation:
Liu X, Lu R, Ding Z, Lyu Z, Li Y and Dong Z (2021) Holocene Environmental Changes Inferred From an Aeolian-Palaeosol-Lacustrine Profile in the Mu Us Desert, Northern China. Front. Earth Sci. 9:799935. doi: 10.3389/feart.2021.799935

INTRODUCTION

The Holocene (from around 11.7 ka BP to the present) may appear as a blink of an eye considering the long history of the Earth, yet it is vitally important to understanding current and recent environmental conditions (Qin, 2011). As an interglacial period, the climate patterns during the Holocene are relatively warm-moist, particularly the ubiquitous and long-term Holocene Megathermal period

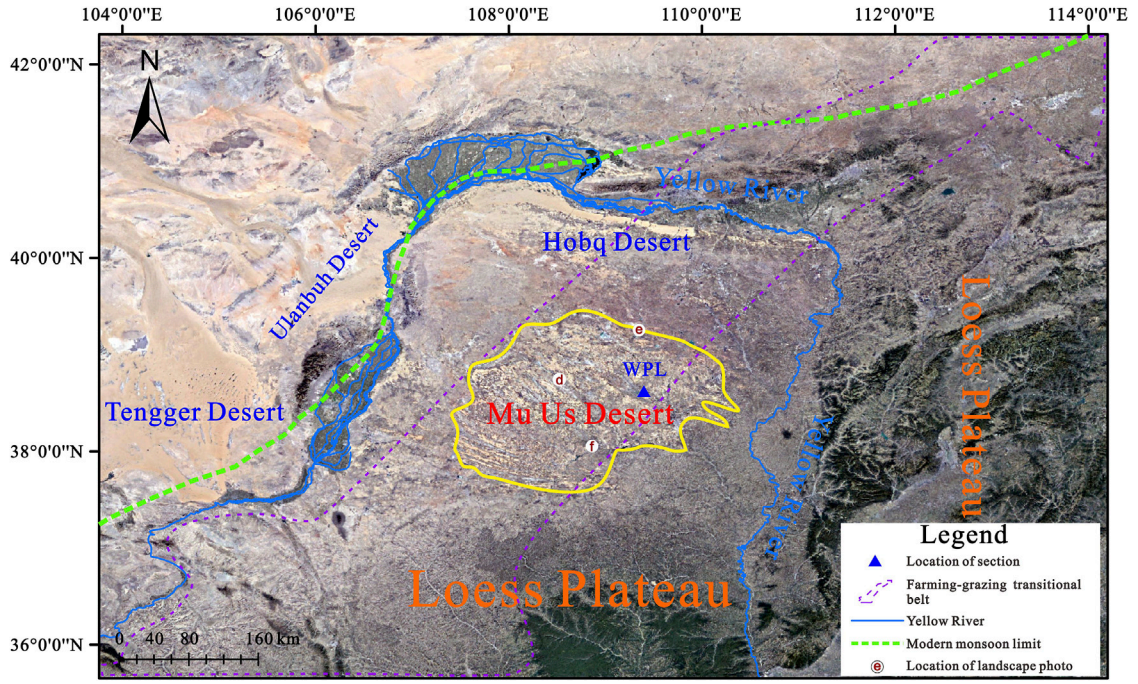

FIGURE 1 | The geographical location of the Mu Us Desert, China. The locations of landscape photo d, e, and f correspond to the picture of **Figures 4D–F**, respectively.

(8.5 ka BP to 3.0 ka BP) (Shi et al., 1994). Previous studies have revealed that this was a prosperous period, with high lake levels (Liu et al., 2018a; Chen et al., 2021), massive glacial thaw (Nesje and Kvamme, 1991; Nesje, 1992), well-developed palaeosol (Lu et al., 2005; Yue et al., 2021), and extensive prehistoric human activities (Nicoll, 2004; Liu et al., 2021). In particular, in ecologically fragile monsoon marginal and agricultural and pastoral interlaced zones, numerous sedimentary profiles or cores have recorded multiple sedimentary facies variations (Zhang et al., 2011; Chen et al., 2015; Shanahan et al., 2015; Liu et al., 2018b; Li et al., 2021). The frequent variations in lacustrine and aeolian activities recorded in individual profiles indicate the quick response and feedback of the regional climatic and environmental changes (Li et al., 2012; Liu et al., 2018a).

The Mu Us Desert in Northern China is located in a desert-loess transitional zone, on the northern margin of the East Asian Summer Monsoon (EASM), within a farming-grazing transitional belt (**Figure 1**). The area is highly sensitive to environmental variation driven by climate change and/or human impacts and is therefore suitable for studying palaeoclimatic and palaeoenvironmental history (Zhou et al., 2002; Ding et al., 2005). Since the 1920s, efforts to understand Holocene palaeoclimate in the Mu Us Desert have found that under the background of climatic variation during the Holocene, aeolian and fluvio-lacustrine deposits coexisted, and the differences that arose concerned the proportion of these different lithologies over time (Liu et al., 2018a), which has been confirmed by various geological records (Ding et al., 2021; Shu et al., 2021). Based on the chronology, lithology, and environmental indices, during the Holocene Climate Optimum period, one or two (perhaps even four) layers of palaeosol and sandy palaeosol were widely developed, corresponding to that the sand dunes were mostly fixed (Gao et al., 2001; Xu Z. et al., 2015; Jia et al., 2015; Zhao S. et al., 2016).

In general, owing to the limits in the distribution area and ideal exposed profiles, together with the frequent meandering Salawusu palaeo-river (a major river in the southern area of Mu Us Desert) (Zhao H. et al., 2016), to date, little attention has been paid to the reconstruction of these sedimentary conditions, especially since an individual profile has identified the presence of multiple sedimentary facies (Zhao H. et al, 2016; Liu et al., 2018b; Jia et al., 2018). Based on extensive field campaigns, a proper section, Wapianliang (WPL), has been found, with aeolian sand, palaeosol, and lacustrine sediments. Therefore, in this paper, we selected the WPL section and used grain size, magnetic susceptibility, soil micromorphology, chemical elements, and lithology analyses to explore the variations in regional depositional environments during the Holocene in the southeastern marginal areas of the Mu Us Desert. Our main objective is to further understand the changes in the regional sedimentary environment during the Holocene.

MATERIAL AND METHODS

Regional Setting

The Mu Us Desert, with a total area of about 39,000 km^2, is located along the margin of a region influenced by the EASM (**Figure 1**),

TABLE 1 | Lithological description of the WPL section.

Unit number	Depth(cm)	Lithology description	Munsell color
A	620–572	Loose medium aeolian sand. Not bottomed	Pale yellow-brown (10YR6/4)
B	572–512	Relatively tight medium and fine lacustrine sand, with sporadic freshwater gastropod fossils	Light gray (2.5Y7/1)
C	512–372	Loose coarse and medium aeolian sand	Light brown (10YR7/3)
D	372–210	Relatively tight medium and fine sandy palaeosol, with sporadic pseudomyceliums. 230–210 and 372–340 cm are the transitional layers	Dark gray-brown (10YR4/2)
E	210–110	Relatively loose fine aeolian sand	Light brown (10YR6/3)
F	110–86	Relatively loose medium weakly developed sandy palaeosol, with one pottery shard	Light brown (10YR6/3)
G	86–0	Loose medium aeolian sand	Pale yellow-brown (10YR6/4)

which dominates the regional climate. The mean annual rainfall is between 250 and 440 mm and the mean annual temperature is between 6.0 and 8.5°C. Warm and humid air brought by the EASM delivers more than 60–70% of the annual precipitation, which falls mainly between June and August (Liu et al., 2018a). The modern vegetation consists mostly of *Artemisia ordosica* Krasch., *Tamarix chinensis* Lour., and *Hippophae rhamnoides* Linn. Regional landscape types are varied, including stabilized, semistabilized, and active sand dunes, grassland, and interlinked sequences of lakes and marshes (Department of Geography of Peking University et al., 1983; Zhou et al., 1996).

Sampling and Laboratory Measurements

An excavation has exposed a stratum in the southeastern margin of the Mu Us Desert, namely section WPL (N38°34′58″, E109°21′39″, altitude 1226 m), which was chosen for study. The WPL section is an aeolian sand-palaeosol-lacustrine sediments sedimentary sequence about 6.20 m thick. The detailed lithological description is presented in **Table 1**.

Three Accelerator Mass Spectrometry (AMS) ^{14}C dates of the organic sediments were obtained from the WPL section. The analyses were made at the Beta Analytic Radiocarbon Dating Laboratory, and details of the pretreatment procedure are given at http://www.radiocarbon.com/pretreatment-carbon-dating.htm#Washes. The AMS ^{14}C dates were converted to calendar ages using the program Calib 7.02 based on the INTCAL 13 calibration (Reimer et al., 2013). In addition, for the lacustrine layer, we collected two samples for Optical Stimulated Luminescence (OSL) dating. The material from the middle part of the sample tube, which had not been exposed to light, were used for equivalent dose (De) measurements. Pure quartz grains 90–125 μm size were extracted using the procedure employed by the OSL Laboratory of the Qinghai Institute of Salt Lakes, Chinese Academy of Sciences. De measurements were conducted using a Risø DA-20 TL/OSL reader equipped with blue diodes (k = 470 ± 20 nm) and a 90Sr/90Y radioactive beta source. The luminescence was detected using a U-340 filter. The material that was possibly exposed to light at each end of the tube was used to measure the concentrations of Uranium (U), Thorium (Th), and Potassium (K) by neutron-activation-analysis (NAA). The water content was measured by weighing the samples before and after drying. Details of the pretreatment procedure of OSL dating samples are presented in Lai and Brückner (2008). Finally, we obtained the boundary ages of the aeolian sand, sandy palaeosol, and the lacustrine deposit units using linear interpolation.

216 samples were collected from the WPL section at 2 or 4 cm intervals for laboratory measurements. The grain size measurements were made using a Mastersizer 2000 with a measurement range of 0.02–2000 μm at the State Key Laboratory of Earth Surface Processes and Resource Ecology, Beijing Normal University (*see* Lu et al. (2015) for a description of the pretreatment procedure). Measurements of magnetic susceptibility were made using a Bartington Instruments MS2 meter and MS2B sensor at the same laboratory, and after air-drying, the samples were disaggregated and packed into 8 cm^3 plastic boxes. The thin sections of the soil sample from 260 cm depth were produced by the Cambrian Geological Technology Limited Company, Langfang City, Hebei Province, and the identification of the soil micromorphology was conducted using a Leica Microscope. The elemental content analyses of samples were made with an Axios wavelength-dispersive X-ray fluorescence spectrometer using a superlong, sharp-pointed ceramic X-ray light tube with a power of 4 kW and a pipe flow of 160 mA at the Key Laboratory of the Desert and Desertification, Northwest Institute of Eco-Environment and Resources, Chinese Academy of Sciences, Lanzhou, China. The pretreatment procedure is presented in Ding et al. (2019).

The Ti/Sr ratio was used to reflect the amount of precipitation indirectly, particularly in the aeolian deposits. Generally, Ti is a stable element, whereas Sr is more active, therefore, the variation in the Ti/Sr ratio depends on the eluviation of Sr (Chen et al., 1999; Liu et al., 2013). The Ratio of Elements (Re) is the ratio of $(K_2O+Na_2O+CaO+MgO)/(Fe_2O_3+MnO_2)$ as proposed by Liu et al. (2002). In Northern China, K, Na, Ca, and Mg are usually concentrated when the climate is dry, while sediments are rich in Fe and Mn when the climate is wet (Guan, 1992).

RESULTS AND DISCUSSION

Patterns of Variation During the Holocene

Chronology

The sandy palaeosol layers contained organic material, which meets the requirements necessary for AMS ^{14}C measurements.

TABLE 2 | ^{14}C dates for the WPL profile.

Sample No	Laboratory No	Depth (cm)	$^{13}C/^{12}C$ ratio	Radiocarbon age (yr BP)	Calendar age (2σ,cal yr BP)
WPL-14C-00	Beta-436306	96–98	−19.9‰	1250 ± 30	1177 ± 96
WPL-14C-02	Beta-436307	230–232	−20.7‰	4210 ± 30	4738.5 ± 110.5
WPL-14C-06	Beta-436308	330–332	−21.6‰	6560 ± 30	7489.5 ± 64.5

TABLE 3 | OSL dates for the WPL profile.

Sample No	Laboratory No	Depth (cm)	U (ppm)	Th (ppm)	K (%)	Moisture (%)	Environmental dose rate (Gy/Ka)	De (Gy)	OSL age (ka)
ISL-LUM2017-93	WPL-OSL-14	490	1.15 ± 0.06	2.44 ± 0.10	2.41 ± 0.07	0	2.79 ± 0.21	27.6 ± 2.1	9.9 ± 1.1
ISL-LUM2017-98	WPL-OSL-17	600	0.68 ± 0.04	2.95 ± 0.11	2.43 ± 0.07	0.01	2.72 ± 0.21	35.4 ± 2.7	13.0 ± 1.4

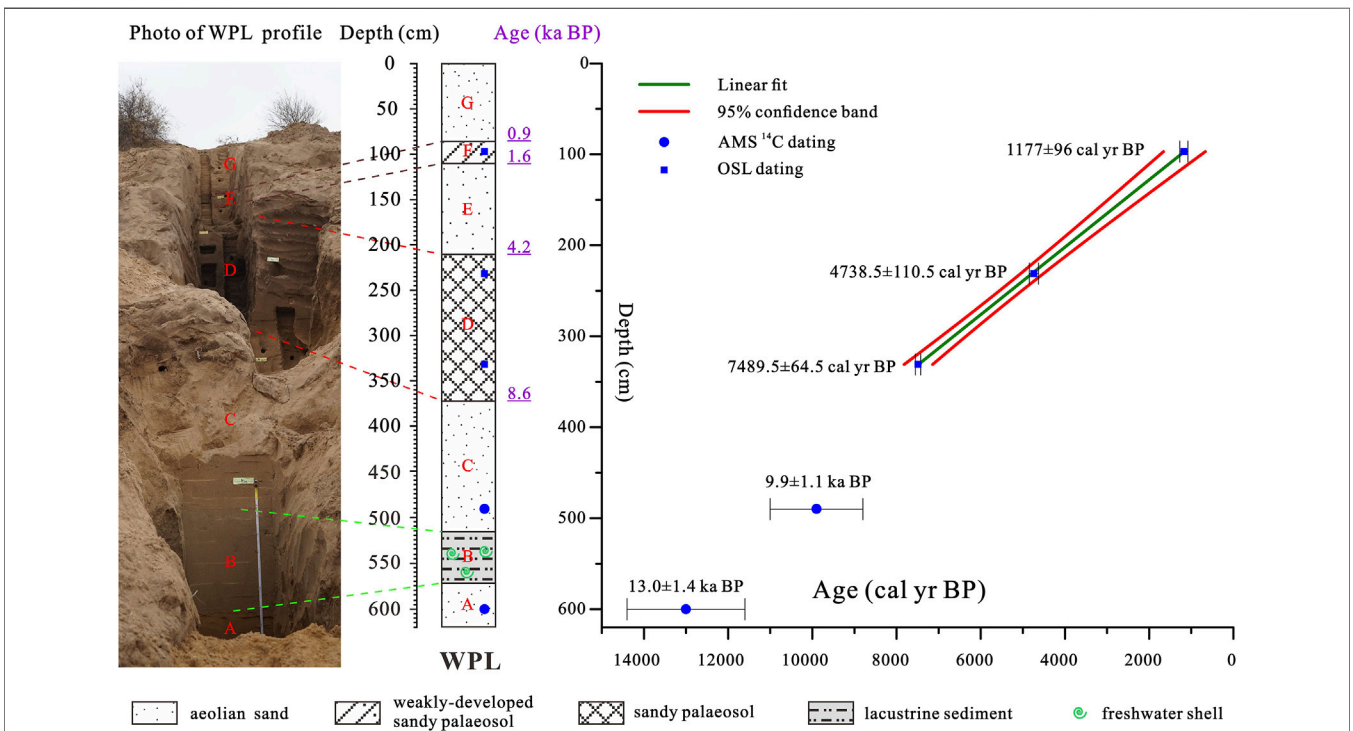

FIGURE 2 | The age-depth model for the WPL profile, based on AMS ^{14}C and OSL ages. 2σ calibrated age or error ranges were shown for each age and the red lines are the 95% confidence interval.

Three samples for dating were chosen and the results for the WPL profile were listed in **Table 2**. All of these dates were obtained from bulk organic matter. For the lower part of the section, to obtain the age of the lacustrine sediment layer, two samples were collected using 4 cm-diameter lucifuge steel tubes for the OSL dating, with the results listed in **Table 3**. Generally, all five ages were in good chronological order. We established a final age model using piecewise linear fitting (**Figure 2**) and the age of the boundary sample was determined by linear interpolation and extrapolation. Because of lack of precise dating data directly derived from the lacustrine layer (Stage B), here we selected the OSL ages from upper and lower aeolian sands to control and

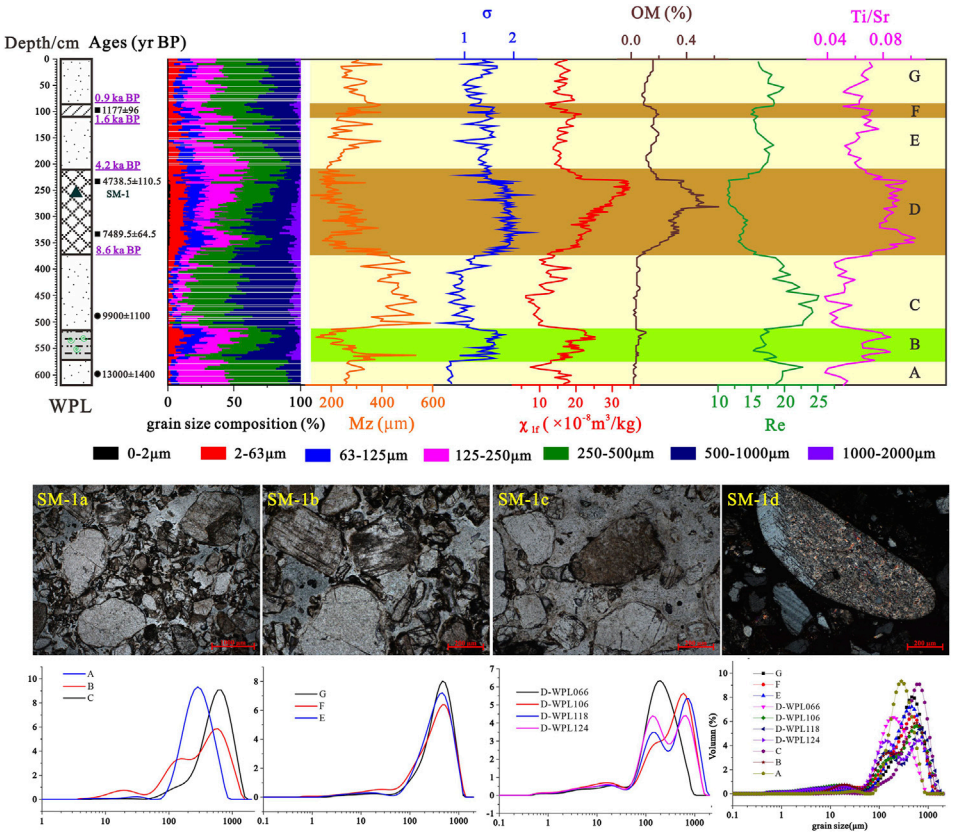

FIGURE 3 | Upper panels: the environmental proxies' variation over the WPL profile. The legend of the profile is same as **Figure 2**. Middle panels: the characteristics of the soil micromorphology of sample SM-1. SM-1a, SM-1b, SM-1c were identified under plane-polarized light and SM-1d was identified under cross-polarized light. The scales are 200 μm. Lower panels: representative grain size frequency distribution curves for the WPL section.

represent the possible development period of the lacustrine sediments Stage B to a certain degree.

Palaeoclimatic Record of the WPL Profile

To summarize the main phases of the site's sedimentary evolution, the record was divided into seven stages, labeled A to G from bottom to top (**Figure 3**).

Stage A. We interpreted the pale yellow-brown aeolian sand layer A to represent the sand of the late glacial period (before 13.0 ± 1.4 ka BP), as indicated by it having the highest medium sand content (47%), the lowest clay and silt contents (0 and 2%), and the best sorting (0.63ϕ, the minimum of all the identified stages). The curve of the grain size frequency distribution for this stage showed a near symmetrical single peak. Meanwhile, the low-frequency magnetic susceptibility (χl_f) and the organic matter content (OM) showed low values (**Figure 3**). Under a same provenance circumstance, the value of χ_{lf} is predominantly affected by climate, particularly precipitation, as characterized by the different degrees of pedogenesis (Tite and Linington, 1975; An et al., 1991; Verosub et al., 1993). The lower values of χ_{lf} and OM mean there was little precipitation, sparse vegetation, and weak pedogenesis.

Considering the geochemical element indices, the value of Ti/Sr was low and Re was high, representing an arid environment with low precipitation. All the selected environmental proxies indicate an aeolian sand-dominated environment, with an arid climate, poor precipitation, and rare vegetation during the late glacial period (before 13.0 ± 1.4 ka BP) in our study area.

Stage B. Between around 13.0 ± 1.4 ka BP and 9.9 ± 1.1 ka BP, the former aeolian sand was succeeded by light gray lacustrine sand, with sporadic freshwater gastropod fossils, which reflects a shallow lake environment. In detail, the grain size parameters exhibit a higher content of silt and very fine sand (13.84%, highest of the whole profile) and worse sorting. The grain size frequency distribution curve for this stage shows three peaks, indicating a mixture of multiple types of interactions between water and wind. For the other indices, the higher χ_{lf} and less obvious crest value of OM indicate the enhancement of the input magnetic materials during this time. In addition, the lower value of Re and higher value of Ti/Sr indicate a relatively humid environment with more precipitation (**Figure 3**). As a whole, we speculate that during this interval, the regional environment existed within a vivifying situation, with lake-dominated conditions and a relatively humid climate, abundant precipitation, and surrounded by lush vegetation at the beginning of the Holocene.

Stage C. For the interval from around 9.9 ± 1.1 ka BP to 8.6 ka BP, the lithology is seen to be typical aeolian sand, characterized by the highest mean grain size (Mz) with medium sand, coarse

sand, and very coarse sand, and better sorting. The grain size frequency distribution curve showed a single peak, similar to Stage A. In addition, the low χ_{lf} value and the near-zero content of OM all indicate an extremely weak degree of pedogenesis and a sparsely vegetated environment. The higher value of Re and lower value of Ti/Sr indicate that during this period, there existed a relatively arid climate, with less precipitation (**Figure 3**).

Stage D. This stage represents the period from between 8.6 ka BP and 4.2 ka BP. The lithology is dark gray-brown sandy palaeosol, with sporadic pseudomyceliums. The Mz of this stage was 243.88 μm, the minimum of all the sedimentary layers, with the highest content of clay (the only one, over 1%) and silt, and the worst sorting. The frequency distribution curve for grain size showed a double peak or three-peak patterns (**Figure 3**, low part, D-WPL066, D-WPL106, D-WPL118, D-WPL124), pointing to the diversity of sources, such as the various processes of pedogenesis. Considering soil micromorphology, sample SM-1 displayed a relatively coarse sand structure, which contained quartz, feldspar, mica, and other lithic minerals, with the total content of silt and clay minerals being less than 10%. In detail, the soil particles were loosely arranged, with few clay minerals. The main quartz was single-crystal quartz (41%), with the development of the secondary enlargement, and the distribution of clay line. Its surface was clean and displayed no cleavage. The feldspar was comprised of alkali feldspar and plagioclase (45%) and developed alteration of micacization and kaolinization. As a whole, all of these characteristics imply a relatively weak degree of pedogenesis during Stage D. Given the expression of the soil character, we called this stage sandy palaeosol. In addition, it shows the highest value of χ_{lf} and OM content, indicating the existence of pedogenesis and a flourishing vegetated environment. Together with the results of the element geochemical index, which saw the lowest value of Re and highest value of Ti/Sr, during this period there existed widely developed palaeosol, with a relatively humid climate, more precipitation, and flourishing vegetation (**Figure 3**). Thereinto, at a depth of between 230 and 210 cm, the transitional layer exhibited obvious transitional characteristics, from the stage D to stage E (**Figure 3**).

Stage E. For the interval from 4.2 ka BP to 1.6 ka BP (Late Holocene), the lithology is light brown aeolian sand. The grain composition mainly consists of medium, fine, and coarse sand (approximatively 80%). The sorting for Stage E is better than for Stage D and the grain size frequency curve mainly showed a typical single-peak pattern, similar to stages A and C. In addition, the lower values of χ_{lf} and OM content indicate a weak degree of pedogenesis and less vegetation. The value of Re sightly increased, together with a lower value of Ti/Sr. These results indicate that during this Late Holocene period, the regional climate was relatively arid, with less precipitation, and less vegetation coverage (**Figure 3**).

Stage F. At this stage (from around 1.6 ka BP to 0.9 ka BP, or around 1.2 ka BP), we obtained an AMS ^{14}C dating age (1177 ± 96 yr cal BP) using organic material. In the weakly developed sandy palaeosol layer, the clay content was relatively high, second to the Stage D sandy palaeosol layer. The grain size frequency distribution curve mainly showed a double peak pattern, and the curve was relatively smooth, implying the weak effect of pedogenesis. The higher values of χ_{lf} and OM content all confirmed the development of soil and the existence of more vegetation. For the geochemistry of elements, the valley value of Ti/Sr and the crest value of Re indicate a relatively humid climate, with more precipitation (**Figure 3**). We, therefore, speculate that Stage F was a period of weakly developed palaeosol.

Stage G. For the top layer, we interpreted the pale yellow-brown aeolian sand to represent the sand of recent millennial deposits (around 0.9 ka BP to the present). Its grain composition was composed of medium, coarse, and fine sand (over 80%), and the frequency distribution curve of the grain size showed a single peak pattern. The lower value of χ_{lf} and OM content, together with the geochemistry results (lower Ti/Sr value and higher value of Re) (**Figure 3**) indicated that after 0.9 ka BP, there existed a relatively arid climate with less precipitation.

Based on these proxies', since the late glacial period, the WPL section with aeolian sand, palaeosol, and lacustrine sediments has documented at least seven stratigraphic cycles, varying between desert and non-desert periods. Generally, for the four desert periods, Stages A, C, E, and G, their mean grain sizes were coarser, sorting was better, the frequency curves had mainly single-peaked forms, and the values of χ_{lf} and OM content were lower, with the combination of elements showing obvious arid climate patterns. Conversely, over the three non-desert periods, which include the lacustrine deposits and sandy palaeosol or weakly developed sandy palaeosol, Stages B, D, and F, their mean grain sizes were finer, sorting was worse, the frequency curves showed double-peaked or multimodal patterns, and the values of χ_{lf} and OM content were higher. Furthermore, the combination of elements showed obvious humid climate patterns.

Development of Regional Sedimentary Conditions Inferred From the WPL Profile and Its Climatic Control

At each stage, the sedimentation reflects the different regional environments, hence, the study of sedimentary facies provides perspective on what the environment could have been at that time. In order to better understand the geomorphic processes and variations in the sedimentary conditions, we considered the possible forcing mechanisms.

Based on the results of **section 3.1.2**, we speculated upon the possible regional sedimentary conditions for each stage. As seen from **Figure 4A**, we considered Stages A, C, E, and G, that is, from before 13.0 ± 1.4 ka BP, from between 9.9 ± 1.1 ka BP to 8.6 ka BP, from 4.2 ka BP to 1.6 ka BP, and from 0.9 ka BP to the present, respectively, to indicate cold and dry desert environments, characterized by strong aeolian activity with coarser grain sizes, better sorting, lower OM content, lower χ_{lf}, and Ti/Sr values, and higher Re values (*see* image **Figure 4D**, which was taken at the hinterland of the modern Mu Us Desert). The emergence or disappearance of aeolian sand was strongly affected by the intensity of the EASM, whether during the Last Glaciation period or the Late Holocene (**Figures 5A–F**). This should be detailly introduced and discussed later.

For Stage B, from around 13.0 ± 1.4 ka BP to 9.9 ± 1.1 ka BP as shown in **Figure 4B**, we speculated that it was a shallow lake environment, which is attributed to a relatively warm and moist

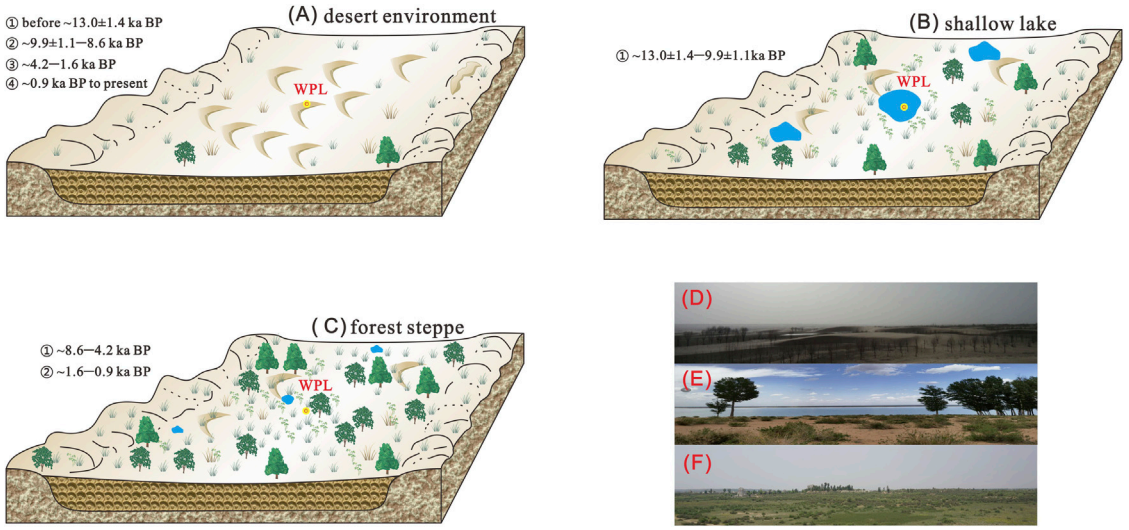

FIGURE 4 | The sketch map of regional sedimentary conditions. **(A)** Desert environment dominated by active dunes. **(B)** Shallow lake environment. **(C)** Forest steppe environment with luxuriant vegetation. Thereinto, the differences between the periods 8.6 ka BP to 4.2 ka BP and from 1.6 ka BP to 0.9 ka BP were influenced by the amount of vegetation in the vicinity; **(D)** landscape photo of a desert environment, which was taken at the hinderland of the modern Mu Us Desert; **(E)** landscape photo of a shallow lake, which was taken at Manai Lake in the modern Mu Us Desert; **(F)** landscape photo of a forest steppe environment, which was taken at Tongwan City in the southern margin of the modern Mu Us Desert.

climate during the Last Deglaciation and early Holocene (Zhou et al., 2002), similar to the landscape shown in **Figure 4E**, showing the area at Manai Lake in the modern Mu Us Desert. As seen from **Figure 5H**, since 15 ka BP, orbital variations have driven changes in summer insolation, which led to thermal contrasts between land and sea (An et al., 2000). The enhanced intensity of monsoons could bring more precipitation (**Figures 5A,C,E,F**), consistent with the lower Re values (**Figure 5B**). On the other hand, it is acknowledged that the lakes or marshes that formed during the Last Deglaciation and early Holocene were related to strong aeolian activity, mainly the formation of blowouts. With regards to blowouts and their relationship to the foundation of lakes, Shen et al. (2005) believed Hongjiannao Lake in the eastern margin of the Mu Us Desert was the result of a wind-erosion lake. Because of the uncertainties in the dating, we can only speculate that within the period between around 13.0 ± 1.4 ka BP to around 9.9 ± 1.1 ka BP, there existed an obvious lake environment stage, as evident by sporadic gastropod fossils. In addition, the rise in temperature (**Figure 5D**) produced meltwater from the permafrost (Xu H. et al., 2015), providing another possible source of lake water. A similar view was expressed by Liu et al. (2018a) and this profile provides new evidence for this idea. In fact, examples of emerging lakes and marshes since 15 ka BP to the early Holocene are very common in our studied area, such as Midiwan (Zhou et al., 2002), Tanyaogou (Jia et al., 2018), and Dishaogouwan Left (Liu et al., 2018b).

Considering Stages D and F, from 8.6 ka BP to 4.2 ka BP and from 1.6 ka BP to 0.9 ka BP, respectively, based on the results of the analysis of the environmental proxies and soil micromorphology, we speculate that these stages indicate a forest steppe environment (**Figure 4C**), with the lithology of sandy palaeosol or weakly developed sandy palaeosol. Therefore, we chose the dense herbal and woody plants symbols in **Figure 4**. The timing of Stages D and F correspond to the Holocene Megathermal and Medieval Warm Period (MWP, 600–1280 AD), with an obvious decrease in the degree of drought (**Figure 4B**). Particularly for Stage D, the soil characteristics are obvious, meaning the fixation of sand dunes, the existence of the process of pedogenesis, and the flourishing of vegetation (Shi et al., 1994; Mason et al., 2009; Xu Z. et al., 2015; Jia et al., 2015). Meanwhile, the suitability of climate is also reflected in these stages having the most precipitation (**Figure 5A**) and higher temperatures (**Figure 5D**) during the middle Holocene. The landscape during this period was close to that shown in **Figure 4F**, which was taken at Tongwan City in the southern margin of the modern Mu Us Desert. We propose that an increased intensity in the EASM was the main reason for the presence of the Holocene Optimum and MWP. The WPL section is mainly located within the positive landform area, therefore, the period of development of the soil corresponds to the lacustrine and sandy peat-dominated period based on the synthesis of variations in hydrological conditions inferred from peat-containing profiles (**Figure 5G**). Therefore, the optimum timing of the climate was mostly similar, i.e., 8.5 to 3.0 ka BP and 8.6 to 4.2 ka BP, respectively. Furthermore, for the return of sandy palaeosol during Stage F, the short-lived enhancement of the summer monsoon might be responsible, with the redness of Qinghai Lake also capturing this returned process (**Figure 5C**).

On the whole, these variations in the sedimentary conditions mentioned above are the products of climatic and environmental changes, which were mainly triggered by the EASM (**Figure 5**). As a result, the alternations between wetting and drying were

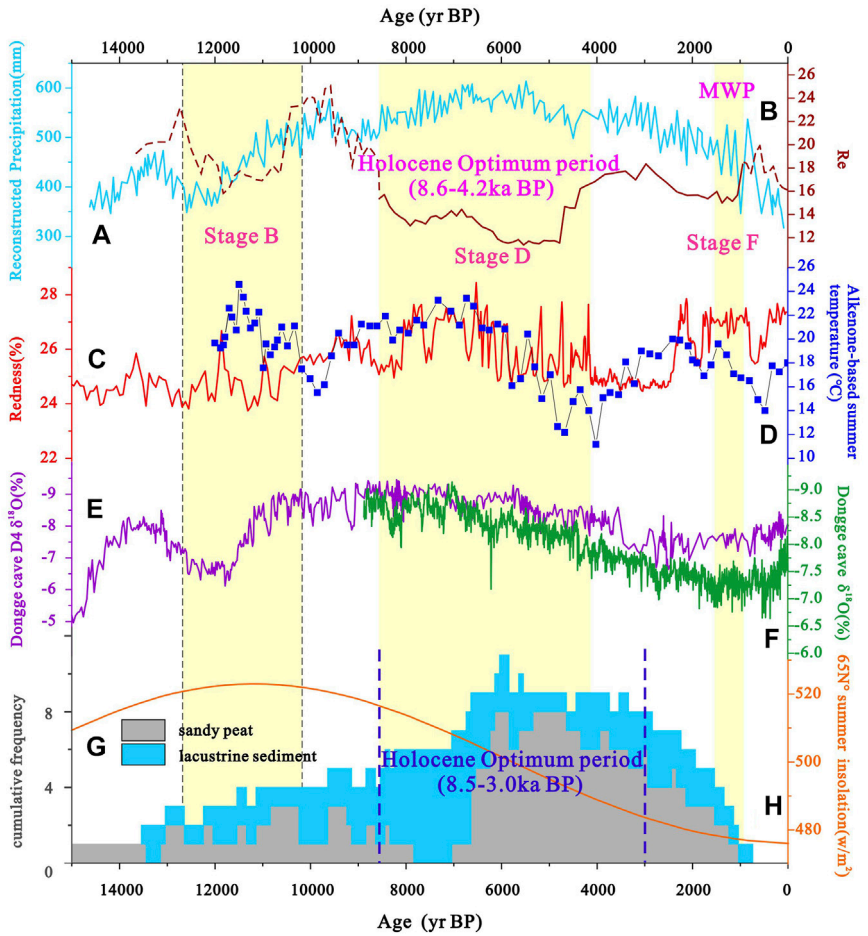

FIGURE 5 | Variations in the Ratio of Elements (Re) representing the degree of drought since the Last Deglaciation period and selected environmental proxies. **(A)** Annual precipitation records from Gonghai Lake, northern China (Chen et al., 2015). **(B)** Re from this paper. **(C)** Redness curve of Qinghai Lake which reflects precipitation (Ji et al., 2005). **(D)** Alkenone-based summer temperature record from Lake Qinghai (Hou et al., 2016). **(E)** Dongge cave stalagmite D4 oxygen isotope record (Dykoski et al., 2005). **(F)** Dongge cave stalagmite oxygen isotope record (Wang et al., 2005). **(G)** Synthesis of variations in hydrological conditions inferred from peat-containing profiles (Liu et al., 2018a). **(H)** Northern Hemisphere summer insolation at 30°N (Berger and Loutre, 1991).

embodied in the identifiable transitions within different landscapes (**Figure 4**).

Regional Comparisons and Environmental Significances

The WPL profile recorded signals of varying temporal scales, from centennial to millennial, characterized by the transition of sedimentary facies and conditions. As mentioned above, in the Mu Us Desert, as a process of the first paludification, peatland development was typically initiated in topographic depressions and in lakeshore and river valley environments (Liu et al., 2018a), as noted in the early-Holocene wetness records widely seen in valleys (Shu et al., 2021). Our studied section belonged to a topographically depressed area, which saw blowout-based shallow lakes forming during Stage B. As the main body of sediments, the Holocene aeolian deposits in our profile were very thick (over 5 m) and lasted for a relatively long time (over 10 ka). The prolonged and prosperous Holocene Optimum, which was characterized by the widely distributed palaeosol and sandy palaeosol stratigraphies, is widely recognized over the Northern China dune fields. In addition to Mu Us Desert region, more sedimentary sequences in the Hulunbuir Sandy Land, the Horqin sandy land, and the Otindag Sandy Land were constantly established (**Figure 6**). Generally, as seen from **Figure 6B**, the light yellow shaded area indicates the age of the middle Holocene palaeosol of the WPL profile and in this regard, it shows that the climate of the middle Holocene in these sandy areas was similarly humid and moist. In particular, between 7.5 and 3.5 ka BP, all the sandy lands in the eastern portion of the desert belt (sand seas and sandy lands) in northern China were stabilized and the intensity of aeolian activity was significantly weakened (Yang et al., 2019). However, previous studies have also demonstrated that the chronological framework about the Holocene palaeosols displayed obvious spatial heterogeneities (Gao et al., 1993; Yang et al., 2019). The differences over time and space could be strongly affected by the East Asian monsoon (Jiang and Liu, 2007). Furthermore, with respect to the reason for these inconsistencies, the instability,

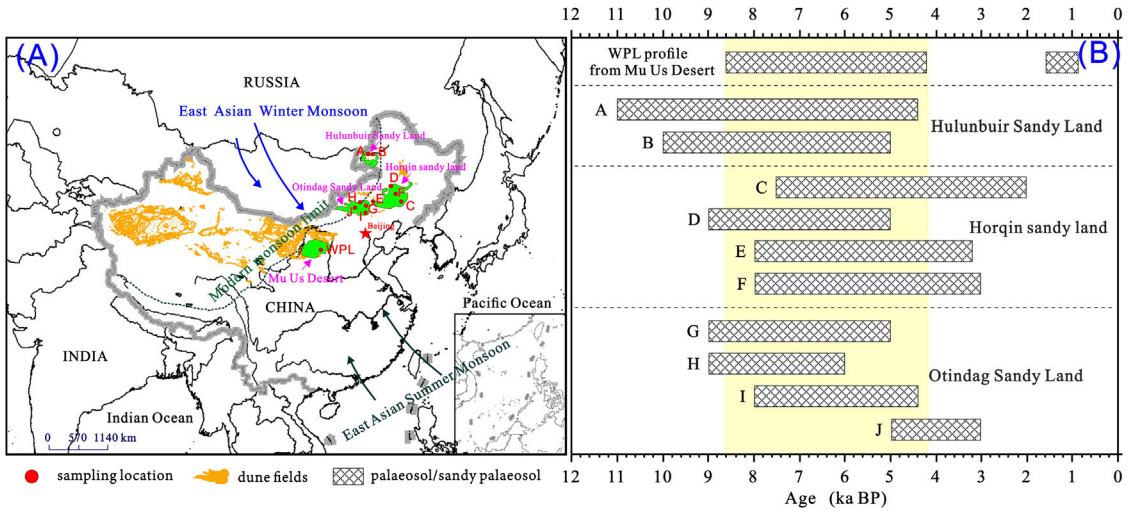

FIGURE 6 | Regional comparisons. **(A)** The location map of our research area, the Mu Us Desert, and a sketch map of the locations of studied points in other sandy lands in Northern China, which were shown in **Figure 6B**. **(B)** The ages of the development of palaeosol/sandy palaeosol in the monsoonal area in Northern China. In detail, A - Li and Sun (2006); B - Yang and Ding (2013); C - Zhao et al. (2007); D - Guo et al. (2017); E - Mu et al. (2016); F - Yang et al. (2012); G - Zhou et al. (2013); H - Jin et al. (2004); I - Gong et al. (2013); J - Yang et al. (2008).

and multiperiod aeolian activities could also impact this region (Jia et al., 2015).

More in-depth palaeoenvironmental studies are required for a full understanding of the relationships between aeolian activity and climate change in northern China (Yang et al., 2019). Profiles such as Wapianliang with aeolian-palaeosol-lacustrine sediments could provide us with more useful information about the varied sedimentary conditions, including the geomorphological processes under Holocene climatic patterns. Furthermore, the study of the transportation and replenishment of materials from centennial to millennial scales may be a way forward in enhancing our understanding of these processes.

CONCLUSION

We have presented a new aeolian-palaeosol-lacustrine profile, Wapianliang, from the Mu Us Desert and have used the results to reconstruct Holocene environmental changes, particularly the sedimentary conditions. The results indicate that since 14 ka BP, this region had experienced seven alternating periods of wetter and dryer climate. Correspondingly, the sedimentary conditions changed from a shallow lake (around 13.0 to 9.9 ka BP), forest steppe environment (around 8.6 ka BP to 4.2 ka BP, and around 1.2 ka BP), and desert environments (the remaining periods). In addition, the variations in depositional environments were mainly triggered by the East Asian monsoon. This section, therefore, provides useful information for enhancing our understanding of the paleoenvironmental evolution of the Mu Us Desert.

DATA AVAILABILITY STATEMENT

The original contributions presented in the study are included in the article/Supplementary Material, further inquiries can be directed to the corresponding author/s.

AUTHOR CONTRIBUTIONS

XL and RL contributed to conception, design of the study and writing of draft of the manuscript. ZDi and ZL conducted investigation and methodology. YL performed the statistical analysis. ZDo provided the funding and resources. All authors contributed to manuscript revision, read, and approved the submitted version.

FUNDING

This study was supported by the National Natural Science Foundation of China (No. 41901094, 41930641, 41330748) and Fundamental Research Funds for the Central Universities (GK202103148).

ACKNOWLEDGMENTS

We thank the editor and anonymous reviewers who have significantly improved this paper. We thank Du Jing for assistance in both field and laboratory, and MJEditor (www.mjeditor.com) for English improvement.

REFERENCES

An, Z., Kukla, G. J., Porter, S. C., and Xiao, J. (1991). Magnetic Susceptibility Evidence of Monsoon Variation on the Loess Plateau of Central China During the Last 130,000 Years. *Quat. Res.* 36 (1), 29–36. doi:10.1016/0033-5894(91)90015-W

An, Z., Porter, S. C., Kutzbach, J. E., Wu, X. H., Wang, S. M., Liu, X. D., et al. (2000). Asynchronous Holocene Optimum of the East Asian Monsoon. *Quat. Sci. Rev.* 19 (8), 743–762. doi:10.1016/S0277-3791(99)00031-1

Berger, A., and Loutre, M. F. (1991). Insolation Values for the Climate of the Last 10 Million Years. *Quat. Sci. Rev.* 10 (4), 297–317. doi:10.1016/0277-3791(91)90033-Q

Chen, C., Tao, S., Zhao, W., Jin, M., Wang, Z., Li, H., et al. (2021). Holocene Lake Level, Vegetation, and Climate at the East Asian Summer Monsoon Margin: A Record from the Lake Wulanhushao Basin, Southern Inner Mongolia. *Palaeogeogr. Palaeoclimatol. Palaeoecol.* 561, 110051. doi:10.1016/j.palaeo.2020.110051

Chen, F., Xu, Q., Chen, J., Birks, H. J. B., Liu, J., Zhang, S., et al. (2015). East Asian Summer Monsoon Precipitation Variability Since the Last Deglaciation. *Sci. Rep.* 5, 1–11. doi:10.1038/srep11186

Chen, J., An, Z., Wang, Y., Ji, J., Chen, Y., and Lu, H. (1999). Distribution of Rb and Sr in the Luochuan Loess- Paleosol Sequence of China During the Last 800 Ka. *Sci. China Ser. D-earth Sci.* 42 (3), 225–232. doi:10.1007/BF02878959

Department of Geography of Peking University (1983). "Commission for Integrated Survey of Natural Resources of Chinese Academy of Sciences," in *Natural Conditions and its Improvement and Utilization in the Mu Us Sandland* (Beijing: Lanzhou Institute of Desert Research of Chinese Academy of Sciences).

Ding, Z. L., Derbyshire, E., Yang, S. L., Sun, J. M., and Liu, T. S. (2005). Stepwise Expansion of Desert Environment Across Northern China in the Past 3.5 Ma and Implications for Monsoon Evolution. *Earth Planet. Sci. Lett.* 237 (1-2), 45–55. doi:10.1016/j.epsl.2005.06.036

Ding, Z., Lu, R., Lyu, Z., and Liu, X. (2019). Geochemical Characteristics of Holocene Aeolian Deposits East of Qinghai Lake, China, and Their Paleoclimatic Implications. *Sci. Total Environ.* 692, 917–929. doi:10.1016/j.scitotenv.2020.136716

Ding, Z., Lu, R., Wang, L., Yu, L., Liu, X., Liu, Y., et al. (2021). Early-Mid Holocene Climatic Changes Inferred from Colors of Eolian Deposits in the Mu Us Desert. *Geoderma* 401, 115172. doi:10.1016/j.geoderma.2021.115172

Dykoski, C., Edwards, R., Cheng, H., Yuan, D., Cai, Y., Zhang, M., et al. (2005). A High-Resolution, Absolute-Dated Holocene and Deglacial Asian Monsoon Record from Dongge Cave, China. *Earth Planet. Sci. Lett.* 233 (1-2), 71–86. doi:10.1016/j.epsl.2005.01.036

Gao, S. Y., Chen, W. N., Jin, H. L., Dong, G. R., Li, B. S., Yang, G. S., et al. (1993). A Preliminary Study on Desert Evolution in the Northwestern Fringe of Monsoon Area, China. *Sci. China, Ser. B* 23 (2), 202–208. doi:10.3321/j.issn:1006-9240.1993.02.005

Gao, S. Y., Wang, G. Y., Ha, S., and Su, Z. Z. (2001). A Case Study on Desert Evolution in the Northwestern Fringe of Monsoon Area, China Since the Last Glacial Epoch. *Quat. Sci.* 21 (1), 66–71. doi:10.3321/j.issn:1001-7410.2001.01.008

Gong, Z., Li, S.-H., Sun, J., and Xue, L. (2013). Environmental Changes in Hunshandake (Otindag) Sandy Land Revealed by Optical Dating and Multi-Proxy Study of Dune Sands. *J. Asian Earth Sci.* 76, 30–36. doi:10.1016/j.jseaes.2013.07.035

Guan, Y. Z. (1992). The Element, Clay Mineral and Depositional Environment in Horqin Sand Land. *J. Desert Res.* 12 (1), 12–18.

Guo, L., Xiong, S., Yang, P., Ye, W., Jin, G., Wu, W., et al. (2018). Holocene Environmental Changes in the Horqin Desert Revealed by OSL Dating and δ 13 C Analyses of Paleosols. *Quat. Int.* 469 (A), 11–19. doi:10.1016/j.quaint.2017.06.048

Hou, J., Huang, Y., Zhao, J., Liu, Z., Colman, S., and An, Z. (2016). Large Holocene Summer Temperature Oscillations and Impact on the Peopling of the Northeastern Tibetan Plateau. *Geophys. Res. Lett.* 43 (3), 1323–1330. doi:10.1002/2015GL067317

Ji, J., Shen, J., Balsam, W., Chen, J., Liu, L., and Liu, X. (2005). Asian Monsoon Oscillations in the Northeastern Qinghai-Tibet Plateau Since the Late Glacial as Interpreted from Visible Reflectance of Qinghai Lake Sediments. *Earth Planet. Sci. Lett.* 233 (1-2), 61–70. doi:10.1016/j.epsl.2005.02.025

Jia, F., Lu, R., Gao, S., Li, J., and Liu, X. (2015). Holocene Aeolian Activities in the Southeastern Mu Us Desert, China. *Aeolian Res.* 19 (B), 267–274. doi:10.1016/j.aeolia.2015.01.002

Jia, F., Lu, R., Liu, X., Zhao, C., Lv, Z., and Gao, S. (2018). Palaeoenvironmental Implications of a Holocene Sequence of Lacustrine-Peat Sediments from the Desert-Loess Transitional Zone in Northern China. *J. Asian Earth Sci.* 156, 167–173. doi:10.1016/j.jseaes.2018.01.030

Jiang, W. Y., and Liu, T. S. (2007). Timing and Spatial Distribution of Mid-holocene Drying Over Northern China: Response to a Southeastward Retreat of the East Asian Monsoon. *J. Geophys. Res.* 112, D241111–D241118. doi:10.1029/2007JD009050

Jin, H. L., Su, Z. Z., Sun, L. Y., Sun, Z., Zhang, H., and Jin, L. Y. (2004). The Holocene Climate Change in the Hunshandake Sandy Land. *Chin. Sci. Bull.* 49 (15), 1532–1536. doi:10.3321/j.issn:0023-074X.2004.15.01210.1007/bf03184307

Lai, Z., and Brückner, H. (2008). Effects of Feldspar Contamination on Equivalent Dose and the Shape of Growth Curve for OSL of Slt-sized Quartz Extracted from Chinese Loess. *Geochronometria* 30, 49–53. doi:10.2478/v10003-008-0010-0

Li, S.-H., Sun, J., and Li, B. (2012). Holocene Environmental Changes in Central Inner Mongolia Revealed by Luminescence Dating of Sediments from the Sala Us River valley. *The Holocene* 22 (4), 397–404. doi:10.1177/0959683611425543

Li, S.-H., and Sun, J. (2006). Optical Dating of Holocene Dune Sands from the Hulun Buir Desert, Northeastern China. *The Holocene* 16 (3), 457–462. doi:10.1191/0959683606hl942rr

Li, Y., Qiang, M., Huang, X., Zhao, Y., Leppänen, J. J., Weckström, J., et al. (2021). Lateglacial and Holocene Climate Change in the NE Tibetan Plateau: Reconciling Divergent Proxies of Asian Summer Monsoon Variability. *Catena* 199, 1050891–1050897. doi:10.1016/j.catena.2020.105089

Liu, B., Jin, H. L., and Sun, Z. (2013). Desert Evolution and Climate Change in the Horqin Sandy Land in Middle and Late Holocene. *J. Desert Res.* 33 (1), 77–86. doi:10.7522/j.issn.1000-694X.2013.00011

Liu, H., Xu, L., and Cui, H. (2002). Holocene History of Desertification Along the Woodland-steppe Border in Northern China. *Quat. Res.* 57 (2), 259–270. doi:10.1006/qres.2001.2310

Liu, X., Lu, R., Du, J., Lyu, Z., Wang, L., Gao, S., et al. (2018a). Evolution of Peatlands in the Mu Us Desert, Northern China, Since the Last Deglaciation. *J. Geophys. Res. Earth Surf.* 123, 252–261. doi:10.1002/2017JF004413

Liu, X., Lu, R., Jia, F., Chen, L., Li, T., Ma, Y., et al. (2018b). Holocene Water-Level Changes Inferred from a Section of Fluvio-Lacustrine Sediments in the Southeastern Mu Us Desert, China. *Quat. Int.* 469 (B), 58–67. doi:10.1016/j.quaint.2016.12.032

Liu, X., Lu, R., Jia, F., Li, X., Li, X., Li, M., et al. (2021). The Strategy and Environmental Significance of Neolithic Subsistence in the Mu Us Desert, China. *Quat. Int.* 574, 68–77. doi:10.1016/j.quaint.2020.12.006

Lu, H., Miao, X., Zhou, Y., Mason, J., Swinehart, J., Zhang, J., et al. (2005). Late Quaternary Aeolian Activity in the Mu Us and Otindag Dune Fields (north China) and Lagged Response to Insolation Forcing. *Geophys. Res. Lett.* 32 (21), 365–370. doi:10.1029/2005GL024560

Lu, R., Jia, F., Gao, S., Shang, Y., Li, J., and Zhao, C. (2015). Holocene Aeolian Activity and Climatic Change in Qinghai Lake Basin, Northeastern Qinghai-Tibetan Plateau. *Palaeogeogr. Palaeoclimatol. Palaeoecol.* 430, 1–10. doi:10.1016/j.palaeo.2015.03.044

Mason, J. A., Lu, H., Zhou, Y., Miao, X., Swinehart, J. B., Liu, Z., et al. (2009). Dune Mobility and Aridity at the Desert Margin of Northern China at a Time of Peak Monsoon Strength. *Geology* 37 (10), 947–950. doi:10.1130/G30240A.1

Mu, Y., Qin, X., Zhang, L., and Xu, B. (2016). Holocene Climate Change Evidence from High-Resolution Loess/paleosol Records and the Linkage to Fire-Climate Change-Human Activities in the Horqin Dunefield in Northern China. *J. Asian Earth Sci.* 121, 1–8. doi:10.1016/j.jseaes.2016.01.017

Nesje, A., and Kvamme, M. (1991). Holocene Glacier and Climate Variations in Western Norway: Evidence for Early Holocene Glacier Demise and Multiple Neoglacial Events. *Geol* 19 (6), 6102–6612. doi:10.1130/0091-7613(1991)0192.3.CO10.1130/0091-7613(1991)019<0610:hgacvi>2.3.co;2

Nesje, A. (1992). Younger Dryas and Holocene Glacier Fluctuations and Equilibrium-Line Altitude Variations in the Jostedalsbre Region, Western Norway. *Clim. Dyn.* 6 (3), 221–227. doi:10.1007/BF00193534

Nicoll, K. (2004). Recent Environmental Change and Prehistoric Human Activity in Egypt and Northern Sudan. *Quat. Sci. Rev.* 23 (5-6), 561–580. doi:10.1016/j.quascirev.2003.10.004

Qin, D. H. (2011). *Preface to the Holocene Climate Change*. Beijing: China Meteorological Press.

Reimer, P. J., Bard, E., Bayliss, A., Beck, J. W., Blackwell, P. G., Ramsey, C. B., et al. (2013). IntCal13 and Marine13 Radiocarbon Age Calibration Curves 0-50,000 Years Cal BP. *Radiocarbon* 55 (4), 1869–1887. doi:10.2458/azu_js_rc.55.16947

Shanahan, T. M., Mckay, N. P., Hughen, K. A., Overpeck, J. T., Otto-Bliesner, B., Heil, C. W., et al. (2015). The Time-Transgressive Termination of the African Humid Period. *Nat. Geosci* 8 (2), 140–144. doi:10.1038/ngeo2329

Shen, J., Wang, Y., Yang, X., Zhang, E., Yang, B., and Ji, J. (2005). Paleosandstorm Characteristics and Lake Evolution History Deduced from Investigation on Lacustrine Sediments-The Case of Hongjiannao Lake, Shaanxi Province. *Chin.Sci.Bull.* 50, 2355–2361. doi:10.1007/BF03183747

Shi, Y. F., Kong, Z. C., Wang, S. M., Tang, L. Y., Wang, F. B., Yao, T. D., et al. (1994). The Climatic Fluctuation and Important Event of Holocene Megathermal in China. *Sci. China B Chem. Life Sci. Earth Sci.* 37 (3), 353–365. doi:10.1360/yb1994-37-3-353

Shu, P., Wang, H., Zhou, W., Ao, H., Niu, D., Wen, X., et al. (2021). Seasonal Rainfall Patterns in Stable Carbon Isotopes in the Mu Us Desert, Northern China During the Early and Middle Holocene. *Clim. Dyn.* 56, 799–812. doi:10.1007/s00382-020-05504-y

Tite, M. S., and Linington, R. E. (1975). Effect of Climate on the Magnetic Susceptibility of Soils. *Nature* 256 (5518), 565–566. doi:10.1038/256565a0

Verosub, K. L., FineSinger, P. M. J., Singer, M. J., and TenPas, J. (1993). Pedogenesis and Paleoclimate: Interpretation of the Magnetic Susceptibility Record of Chinese Loess-Paleosol Sequences. *Geol* 21 (11), 10112–11014. doi:10.1130/0091-7613(1993)021<1011:PAPIOT>2.3.CO10.1130/0091-7613(1993)021<1011:papiot>2.3.co;2

Wang, Y., Cheng, H., Edwards, R. L., He, Y., Kong, X., An, Z., et al. (2005). The Holocene Asian Monsoon: Links to Solar Changes and North Atlantic Climate. *Science* 308 (5723), 854–857. doi:10.1126/science.1106296

Weijian, Z., Donahue, D. J., Porter, S. C., Jull, T. A., Xiaoqiang, L., Stuiver, M., et al. (1996). Variability of Monsoon Climate in East Asia at the End of the Last Glaciation. *Quat. Res.* 46 (3), 219–229. doi:10.1006/qres.1996.0062

Xu, H., Yeager, K. M., Lan, J., Liu, B., Sheng, E., and Zhou, X. (2015a). Abrupt Holocene Indian Summer Monsoon Failures: A Primary Response to Solar Activity? *The Holocene* 25 (4), 677–685. doi:10.1177/0959683614566252

Xu, Z., Lu, H., Yi, S., Vandenberghe, J., Mason, J. A., Zhou, Y., et al. (2015b). Climate-driven Changes to Dune Activity During the Last Glacial Maximum and Deglaciation in the Mu Us Dune Field, North-central China. *Earth Planet. Sci. Lett.* 427, 149–159. doi:10.1016/j.epsl.2015.07.002

Yang, L.-R., and Ding, Z.-L. (2013). Expansion and Contraction of Hulun Buir Dunefield in North-eastern China in the Last Late Glacial and Holocene as Revealed by OSL Dating. *Environ. Earth Sciearth Sci.* 68 (5), 1305–1312. doi:10.1007/s12665-012-1828-3

Yang, L., Wang, T., Zhou, J., Lai, Z., and Long, H. (2012). OSL Chronology and Possible Forcing Mechanisms of Dune Evolution in the Horqin Dunefield in Northern China Since the Last Glacial Maximum. *Quat. Res.* 78 (2), 185–196. doi:10.1016/j.yqres.2012.05.002

Yang, X., Liang, P., Zhang, D., Li, H., Rioual, P., Wang, X., et al. (2019). Holocene Aeolian Stratigraphic Sequences in the Eastern Portion of the Desert belt (Sand Seas and sandy Lands) in Northern China and Their Palaeoenvironmental Implications. *Sci. China Earth Sci.* 62 (8), 1302–1315. doi:10.1007/s11430-018-9304-y

Yang, X., Zhu, B., Wang, X., Li, C., Zhou, Z., Chen, J., et al. (2008). Late Quaternary Environmental Changes and Organic Carbon Density in the Hunshandake Sandy Land, Eastern Inner Mongolia, China. *Glob. Planet. Change* 61 (1-2), 70–78. doi:10.1016/j.gloplacha.2007.08.007

Yue, D.-P., Zhao, J.-B., Ma, Y.-D., Cao, J.-J., Li, Y.-H., Ma, A.-H., et al. (2021). Mid-Holocene Soil Water and Vegetation in the Xi'an Area of the Southern Chinese Loess Plateau. *Geoderma* 383, 1148021–1148029. doi:10.1016/j.geoderma.2020.114802

Zhang, J., Jia, Y., Lai, Z., Long, H., and Yang, L. (2011). Holocene Evolution of Huangqihai Lake in Semi-arid Northern China Based on Sedimentology and Luminescence Dating. *The Holocene* 21 (8), 1261–1268. doi:10.1177/0959683611405232

Zhao, H., Sheng, Y., Li, B., and Fan, Y. (2016a). Holocene Environment Changes Around the Sara Us River, Northern China, Revealed by Optical Dating of Lacustrine-Aeolian Sediments. *J. Asian Earth Sci.* 120, 184–191. doi:10.1016/j.jseaes.2016.02.002

Zhao, H., Lu, Y., and Yin, J. (2007). Optical Dating of Holocene Sand Dune Activities in the Horqin Sand-fields in Inner Mongolia, China, Using the SAR Protocol. *Quat. Geochronol.* 2 (1-4), 29–33. doi:10.1016/j.quageo.2006.03.008

Zhao, S., Xia, D., Jin, H., Jia, J., Li, G., Gao, F., et al. (2016b). Long-term Weakening of the East Asian Summer and Winter Monsoons During the Mid- to Late Holocene Recorded by Aeolian Deposits at the Eastern Edge of the Mu Us Desert. *Palaeogeogr. Palaeoclimatol. Palaeoecol.* 457, 258–268. doi:10.1016/j.palaeo.2016.06.011

Zhou, W. J., Dodson, J., Head, M. J., Li, B. S., Hou, Y. J., Lu, X. F., et al. (2002). Environmental Variability within the Chinese Desert-Loess Transition Zone Over the Last 20000 Years. *The Holocene* 12 (1), 107–112. doi:10.1191/0959683602hl525rr

Zhou, Y. L., Lu, H. Y., Zhang, X. Y., and Yi, S. W. (2013). Changes of the Border of Hunshandake (Otindag) Sand Field (Northern China) During the Last Glacial Maximum and Holocene. *Quat. Sci.* 33 (2), 228–242. doi:10.3969/j.issn.1001-7410.2013.02.04

Conflict of Interest: The authors declare that the research was conducted in the absence of any commercial or financial relationships that could be construed as a potential conflict of interest.

Publisher's Note: All claims expressed in this article are solely those of the authors and do not necessarily represent those of their affiliated organizations, or those of the publisher, the editors and the reviewers. Any product that may be evaluated in this article, or claim that may be made by its manufacturer, is not guaranteed or endorsed by the publisher.